



Measurement of the phonon mean free path spectrum in silicon membranes at different temperatures using arrays of nanoslits

Roman Anufriev ^{*}*Institute of Industrial Science, The University of Tokyo, Tokyo 153-8505, Japan*Jose Ordonez-Miranda *Institut Prime, CNRS, Université de Poitiers, ISAE-ENSMA, F-86962, Futuroscope, Chasseneuil, France*Masahiro Nomura *Institute of Industrial Science, The University of Tokyo, Tokyo 153-8505, Japan*

(Received 24 October 2019; revised manuscript received 13 February 2020; accepted 14 February 2020; published 2 March 2020)

Knowledge of the phonon mean free path (MFP) holds the key to understanding the thermal properties of materials and nanostructures. Although several experiments measured the phonon MFP in bulk silicon, MFP spectra in thin membranes have not been directly measured experimentally yet. In this work, we experimentally probe the phonon MFP spectra in suspended silicon membranes. First, we measure the thermal conductivity of membranes with arrays of slits at different temperatures. Next, we develop a fully analytical procedure to extract the accumulated thermal conductivity as a function of the MFP. The measured phonon MFP in 145-nm-thick membranes with the surface roughness of 0.2 nm is shorter than that in bulk due to the scattering at the membrane boundaries. At room temperature, the phonon MFP does not exceed 400 nm. However, at 4 K, the MFP becomes longer, and some phonons can travel ballistically for up to one micrometer. These results thus shed light on the long-lasting question of the range of ballistic phonon transport at different temperatures in nanostructures based on silicon membranes.

DOI: [10.1103/PhysRevB.101.115301](https://doi.org/10.1103/PhysRevB.101.115301)

I. INTRODUCTION

Understanding heat conduction in semiconductors is crucial for solving heat dissipation problems in modern microelectronics. The thermal properties of semiconductors are largely defined by the spectral quantity called phonon mean free path (MFP)—the average distance that a phonon can travel between scattering events. For the practical applications in thermal engineering, researchers use the cumulative MFP spectra that show how much phonons with a given MFP contribute to the total thermal conductivity.

In the past few years, cumulative MFP spectra have been studied in various bulk materials [1–7]. However, modern microelectronic devices, such as micro- and nanoelectromechanical systems (MEMS and NEMS), often rely on thin films and membranes rather than on bulk materials. In thin two-dimensional structures, phonons experience additional scattering on the top and bottom surfaces [8–10]. Such surface scattering events should limit the phonon MFP in membranes as compared to bulk material [11], thus reducing the thermal conductivity and limiting the ballistic heat conduction. Indeed, the experimentally measured thermal conductivity of thin membranes is consistent with the MFP spectrum in bulk, assuming that the spectrum is limited by the membrane thickness [4].

To directly obtain the phonon MFP spectrum in membranes, researchers used various simulation methods [10–12]. However, no experimental study attempted direct measurements of the phonon MFP spectra of thin membranes because setting up an MFP probing experiment on suspended membranes is challenging. Recently, Hao *et al.* [13] proposed a seminumerical procedure to extract accumulated MFP spectra from the thermal conductivity measured on membranes with arrays of narrow slits with varied width of the passage.

In this work, we apply and extend this method to extract phonon MFP spectra from experimental data under a fully analytical approach. First, we measure the thermal conductivity of membranes with slits at different temperatures. Then we use the improved analytical method to extract MFP spectra from our experimental data. The cumulative MFP spectra show how the MFPs in a thin membrane differ from that in bulk and increase as the temperature is decreased.

II. METHODS

A. Measurement technique

The thermal conductivity of our samples was measured using the micro time-domain thermoreflectance method (μ TDTR). In this all-optical method, pulses of the pump laser periodically heat an aluminum pad in the center of the samples, as shown in Fig. 1(a), while the continuous-wave probe beam measures the reflectance of the pad. The

*anufriev@iis.u-tokyo.ac.jp

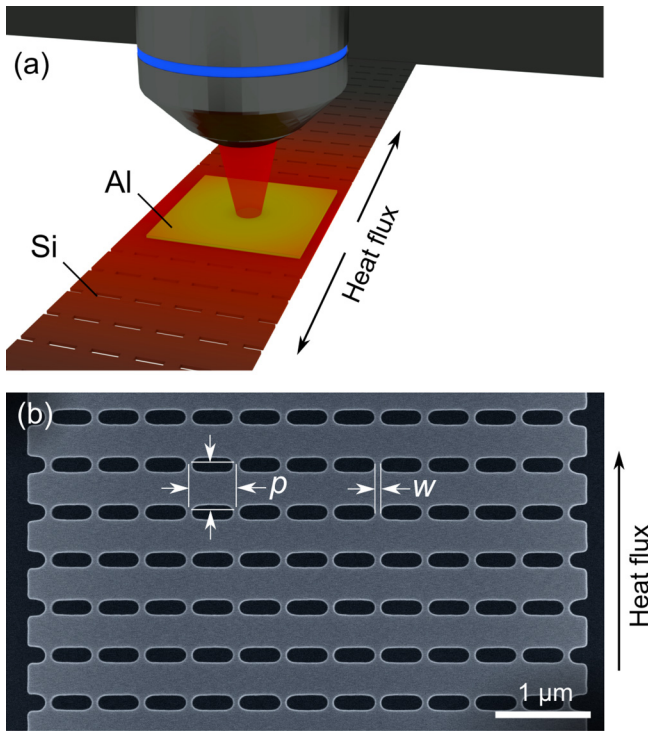


FIG. 1. (a) Scheme of the experimental setup showing the laser beams focused via an optical objective on the suspended bridge. (b) Scanning electron microscope image of a typical sample under investigation.

reflectance of the pad is proportional to its temperature via the thermoreflectance coefficient. Thus, the method allows measuring the gradual decrease in temperature as heat dissipates from the metal pad after each pulse of the pump beam. Exponential fitting $\exp(-t/\tau)$ of this temperature decrease yields the thermal decay time (τ)—the characteristic time of heat dissipation through the bridge supporting the aluminum pad.

The thermal conductivity was extracted from the measured decay time by simulating the same experiment using the finite-element method. In contrast with our previous works [26], here we simulate the membranes without slits and thus extract the effective thermal conductivity, i.e., thermal conductivity without taking into account material removal. In the simulations, the thermal conductivity assigned to the membrane serves as a free parameter, whereas heat capacity is equal to that of bulk silicon at the corresponding temperature. Thus, by varying the thermal conductivity, we can always obtain a value at which the simulation reproduces the experimentally measured cooling curve. More details on this experimental method can be found in our previous work [14].

B. Sample fabrication

Our samples were fabricated using the standard top-down fabrication methods on a silicon-on-insulator wafer. The wafer had a top 145-nm-thick monocrystalline silicon layer with atomically smooth ($\sigma = 0.2$ nm) top and bottom surfaces

[15,16]. First, we deposited aluminum pads on the surface of silicon. Next, we used electron-beam lithography and reactive ion etching to draw and etch the pattern around the aluminum pads and thus create a bridge with the arrays of slits and the aluminum pad in the middle. Finally, we exposed the wafer to the vapor of hydrofluoric acid to remove the sacrificial SiO_2 layer under the bridge and suspend the structure. To avoid the formation of native oxide that might affect the surface phonon scattering [17,18], the samples were placed into the low-pressure cryostat right after the oxide etching. More details on the fabrication process can be found in our previous work [19].

Figure 1(b) shows a typical sample consisting of a 145-nm-thick membrane with arrays of 150-nm-wide slits. To study how the MFP analysis would depend on the scale of the slit array, we fabricated two sets of samples with periods in both directions (p) of the slit arrays equal to 500 and 1000 nm. The roughness of the sidewall of the slits is estimated to be more than 2 nm. Thus we assume that the surface is purely diffusive, at least at 150 and 300 K. However, this assumption may not be entirely correct at the temperature of 4 K, where phonon wavelengths become long enough for nondiffusive surface scattering, and the data at 4 K should be considered with caution.

To obtain an MFP spectrum, we must measure the thermal conductivity values on samples with different widths of passage between the slits (w). Thus, for each period, we prepared samples with different widths of the passage. To ensure the accuracy of our measurements, we fabricated and measured three copies of each sample. The reported thermal conductivity is then obtained as an average of three independent measurements with the error bars showing the standard deviation.

C. Mean free path analysis

To extract the MFP cumulative function from the measured effective thermal conductivity, we use the approach developed by Hao *et al.* [13]. This approach is based on the assumption that phonon scattering on the membrane boundaries suppresses the thermal conductivity independently from the phonon scattering on the slits. This assumption is generally correct only for very thick membranes [20]. For our 145-nm-thick membrane, this assumption still does not introduce any significant error at temperatures of 150 and 300 K but can lead to up to 10% error for the data obtained at 4 K.

Based on some analytical considerations, Hao *et al.* [13] showed that the effective thermal conductivity $\kappa_{\text{eff}}(w)$ normalized by the thermal conductivity κ_{ref} of a membrane without slits is related to the MFP cumulative function $F(\Lambda)$ by

$$\frac{\kappa_{\text{eff}}}{\kappa_{\text{ref}}} = H(w)a(w) \int_0^\infty \frac{F(\Lambda)d\Lambda}{[1 + a(w)\Lambda]^2}, \quad (1)$$

where $a(w) = (4p/3L) \times H(w)/(w \times A)$. Here, L is the length of the system, which in our case is the same as the period p , in other words, the length of one period in the heat flux direction. The function $H(w)$ accounts for the reduction of material volume, i.e., the bulk porosity effect that causes the

suppression of thermal conduction simply due to the material removal and bending of the heat flux lines. We obtained the $H(w)$ function for our samples by simulating a unit cell of the structure using the finite-element method implemented in COMSOL MULTIPHYSICS.

The factor A accounts for the difference between an analytically calculated [13] limiting dimension for a single narrow slit (L_c) and the generally unknown limiting dimension of the experimentally studied array of slits (L_c^*). Hua and Cao [21] showed that the difference in the limiting dimension for two-dimensional arrays of holes can be accounted for by a geometrical factor (A) as $L_c^* = A \times L_c$. To obtain this factor, we applied the Callaway-Holland model, in which the relaxation time of the boundary scattering was used as a free parameter (Appendix A). Thus, we found $A = 0.7$ and 0.6 for arrays with $p = 500$ and 1000 nm, respectively.

To improve the computational efficiency of the original seminumerical approach [13], we propose to simplify the method and use an analytical expression for the $F(\Lambda)$ function. Indeed, as $F(\Lambda)$ monotonically increases with Λ between zero and unity, its general behavior can be expressed as [22]

$$F(\Lambda) = -\frac{\Lambda}{\alpha} W_0 \left[-\frac{\alpha}{2\Lambda} \exp\left(-\frac{\alpha}{\Lambda}\right) \operatorname{erfc}\left(\frac{\Lambda_0 - \Lambda}{\sqrt{2}\beta}\right) \right], \quad (2)$$

where W_0 is the Lambert function of order zero, erfc is the complementary error function, and α , β , and Λ_0 are fitting parameters. Appendix B details the rationale for using Eq. (2) and tolerance to the fitting parameters. Inserting Eq. (2) into Eq. (1), we obtain

$$\frac{\kappa_{\text{eff}}}{\kappa_{\text{ref}}} = H(w) \int_0^1 G(x, \alpha', \beta', \gamma') dx, \quad (3)$$

where $\alpha' = \alpha a(w)$, $\beta' = \beta a(w)$, and $\gamma' = 1 + \Lambda_0 a(w)$ are nondimensional parameters, $x = [1 + a(\omega)\Lambda]^{-1}$, and

$$G(x, \alpha', \beta', \gamma') = \frac{1-x^{-1}}{\alpha'} W_0 \left[-\frac{\alpha'}{2(1-x^{-1})} \exp\left(\frac{\alpha'}{1-x^{-1}}\right) \times \operatorname{erfc}\left(\frac{\gamma' - x^{-1}}{\sqrt{2}\beta'}\right) \right]. \quad (4)$$

The nondimensional equations (3) and (4) are used to determine α , β , and Λ_0 by fitting the experimentally measured $\kappa_{\text{eff}}(w)/\kappa_{\text{ref}}$ values. To illustrate this method, Fig. 2 shows the data reported by Hao *et al.* [13] and the fit that we obtained using Eq. (3). To justify the use of the generalized analytical form of $F(\Lambda)$, we also compare the extracted MFP spectra. The inset of Fig. 2 shows that our analytical approach yields an accurate match of the MFP spectrum obtained numerically by Hao *et al.* [13].

III. RESULTS AND DISCUSSION

Figure 3 shows the effective thermal conductivity (κ_{eff}) of samples with periods of 500 and 1000 nm measured at 4, 150, and 300 K and normalized by the thermal conductivity of membranes without slits (κ_{ref}). The membrane thermal conductivity was 0.044, 110.3, and 71.3 $\text{W m}^{-1} \text{K}^{-1}$ at 4, 150, and 300 K, respectively. These values are consistent with the

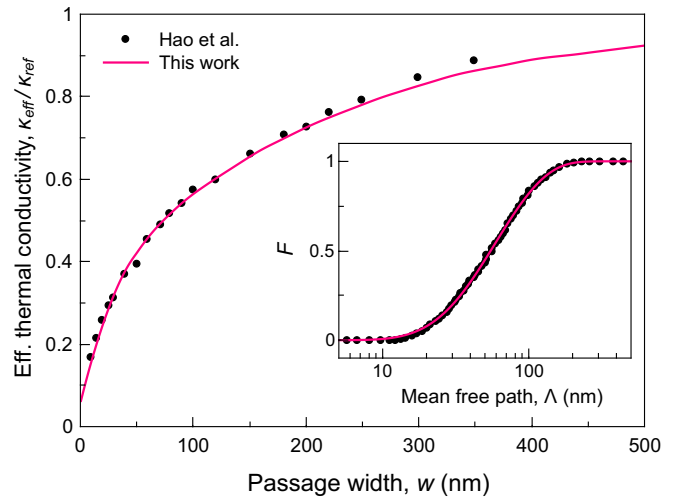


FIG. 2. Comparison of the predictions of the original seminumerical approach proposed by Hao *et al.* [13] with those of our fully analytical method. Our Eq. (3) fits well the data obtained via simulations in [13], and the extracted MFP accumulation function (inset) agrees with that extracted by using the seminumerical approach.

theoretically predicted $100 \text{ W m}^{-1} \text{K}^{-1}$ [10] at 150 K and $60\text{--}75 \text{ W m}^{-1} \text{K}^{-1}$ [10–12] at 300 K.

The thermal conductivity increases proportionally with the width of passage between the slits (w).

These curves essentially reflect the dependence of thermal conductivity on the phonon MFP as wider passages allow for longer free flights of phonons. As such, this dependence lies at the core of our method. The slope of this dependence naturally lowers as the temperature is decreased. Indeed, at lower temperatures, phonons tend to have longer MFP [2–4]. Thus, passages of the same width cut a more substantial part of the MFP spectrum at 4 K than at 300 K. This effect allows probing MFP spectra at different temperatures.

Fitting the curves in Fig. 3 using Eq. (3), we obtained the nondimensional parameters α , β , and Λ_0 and used them to reconstruct the thermal conductivity accumulation functions $F(\Lambda)$. Figure 4 shows the extracted cumulative MFP spectra $F(\Lambda)$ for samples with periods of 500 and 1000 nm at 4, 150, and 300 K. The curves obtained for two different periods are reasonably similar. The agreement between two data sets is not surprising, as both sample sets have passage widths (w) covering most of the range of probed MFPs. For this reason, the best agreement between two data sets is obtained at 150 K, when both sample sets cover nearly the entire MFP range. On the contrary, some disagreement occurs at 4 and 300 K, as we expect a better result from samples with wider and narrower passages, correspondingly.

At room temperature, the range of measured MFPs spans from 10 to 400 nm. This range is more than twice shorter than that in bulk silicon, where phonons with MFP longer than 800 nm may contribute to 37%–47% of the thermal conductivity [10,23]. Such a short MFP explains why heat conduction in membrane-based structures usually appears diffusive at 300 K [24–26]. For example, recent experiments could not detect any signs of phonon interference in phononic crystals [27,28] or nanomeshes [29] with the periodicity of a few

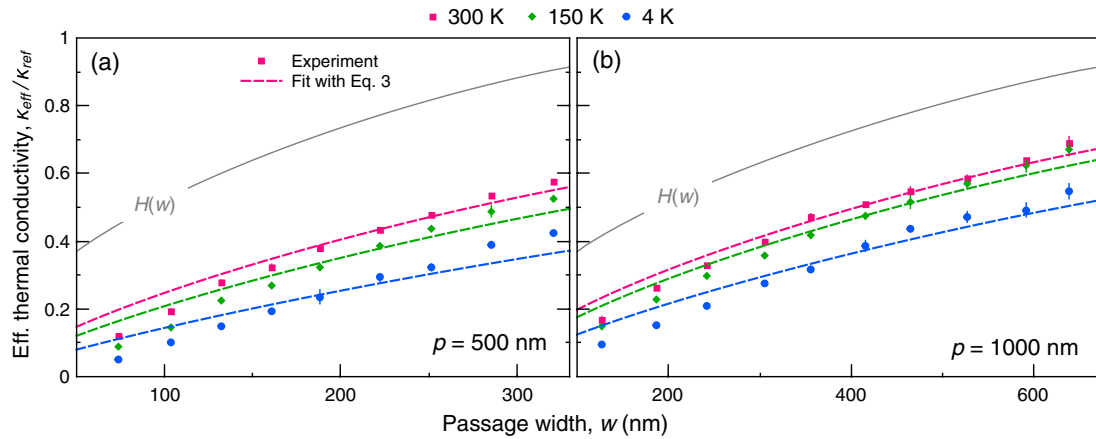


FIG. 3. Normalized effective thermal conductivity of membranes with arrays of slits having periods of (a) 500 nm and (b) 1000 nm measured at 4, 150, and 300 K. Dashed lines show the best fits of the data with Eq. (3). Solid lines show the volume reduction functions $H(w)$.

hundred nanometers. Similarly, experiments on 400-nm-long nanowires could not detect any signs of ballistic phonon transport at this scale [19]. However, this MFP range contrasts with observations by Johnson *et al.* [30], who measured quasiballistic heat conduction in silicon membranes at room temperature at length scales up to $5 \mu\text{m}$.

The measured cumulative MFP spectra generally resemble the theoretical predictions for membranes at room temperature [10–12]. However, in contrast with our results, the simulations tend to predict significant contribution (10%–30%) from phonons with the MFP longer than 400 nm. Moreover, simulations by Wang and Huang [10] suggest that up to 70% of the total thermal energy is carried by phonons with the MFP shorter than 100 nm in 130-nm-thick membranes, while our measurements show only up to 50% contribution. The discrepancy with this prediction might be due to the purely diffusive surface scattering assumed in the simulations [10]. Indeed, recent experiments suggest that the scattering is partly specular even at room temperature [31].

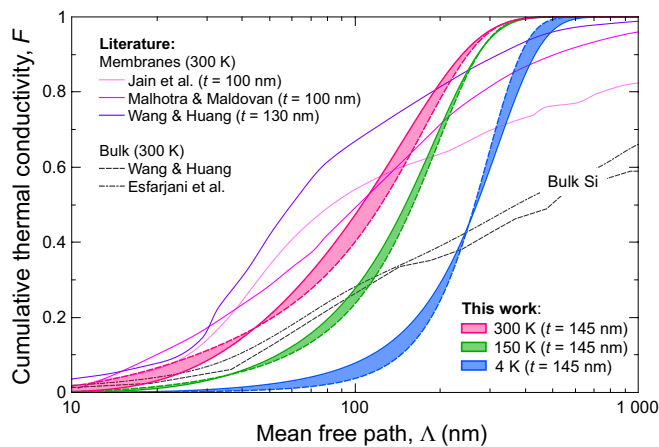


FIG. 4. Cumulative thermal conductivity of silicon membranes as a function of the phonon MFP obtained for samples with periods of 500 nm (solid lines) and 1000 nm (dashed lines) at 4, 150, and 300 K. For comparison, curves theoretically obtained in the literature for membranes of different thicknesses [10–12] and the bulk [10,23] are also shown.

As we decrease the temperature, the MFPs become longer. At 150 K, the short side of the MFP spectrum shifts towards longer MFPs so that 70% of heat is carried by phonons with MFP longer than 100 nm. Yet, the longest MFPs remain below 400 nm, which is much shorter than the MFP in bulk silicon at this temperature (10^{-1} – $10^3 \mu\text{m}$) [7]. At 4 K, almost all the phonons have a MFP longer than 100 nm but still shorter than 600 nm. Thus, the phonon MFP in membranes remains strongly suppressed as compared to that in bulk, even at 4 K, when the surface phonon scattering should be predominantly specular [19].

Nevertheless, MFPs in the 100–600 nm range are sufficiently long for multiple elastic reflections of phonons, provided that reflecting surfaces are smooth enough. Such multiple reflections might cause phonon interference in the periodic membrane-based nanostructures with surface quality higher than in the present work. Indeed, low-temperature experiments recently showed the various effects occurring due to the long MFP: quasiballistic conduction [14,32], partly [27] or fully [33,34] coherent heat conduction in phononic crystals, ballistic heat guiding, and focusing [16]. Moreover, the measured 100–600 nm range of phonon MFPs at 4 K is consistent with the strength of ballistic heat conduction measured in silicon nanowires [19], where roughly 25% of phonons had MFPs longer than 800 nm and 55% had MFPs shorter than 400 nm at 4 K.

IV. CONCLUSIONS

We have experimentally probed the phonon MFP spectra in 145-nm-thick silicon membranes with surface roughness of 0.2 nm at different temperatures. Our experiments and subsequent analysis showed that the phonon MFPs in membranes are much shorter than in bulk due to the phonon surface scattering induced by the top and bottom boundaries of the membrane. At room temperature, 90% of heat is carried by phonons with MFPs in the 30–300-nm range. At lower temperatures, MFPs become longer as internal and diffuse scattering processes weaken. The MFPs measured at 4 K are in the 100–600-nm range, which is wide enough to involve ballistic or coherent heat conduction in realistic membrane-based nanostructures. These data explain why

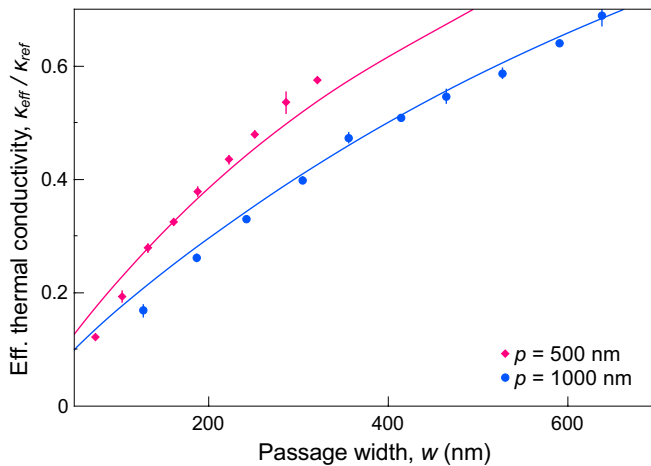


FIG. 5. Thermal conductivity for $p = 500$ and 1000 nm experimentally measured at 300 K and fitted with the Callaway-Holland model.

room-temperature heat conduction appears diffusive at the length scales of several hundreds of nanometers, whereas low-temperature heat conduction at this scale becomes quasiballistic. In the future, the proposed methods could be applied to investigate the MFP spectra in materials with long bulk MFPs (BAs, SiC, or BN), which will help to find better materials for future microelectronics.

ACKNOWLEDGMENTS

This work was supported by JST, PRESTO Grant No. JPMJPR19I1, CREST Grant No. JPMJCR19Q3, and Kakenhi Grants No. 15H05869, No. 17H02729, and No. 18K14078.

APPENDIX A

Assuming that $L_c^* = A \times L_c$ [21], we can extract the geometrical factor A by fitting the experimentally measured thermal conductivity to the Callaway-Holland model, described in our previous work [35]. Here, we used the relaxation time representing the surface scattering (τ_s) as a fitting parameter. Taking into account that L_c for an ideal case [13] is essentially $L_c = 3w/[4H(w)]$, we can write the relaxation time as $\tau_s = A \times L_c/v$, where v is the phonon group velocity. Thus, using the geometrical factor A as the only fitting parameter, we obtained the best fits with $A = 0.7$ and 0.6 for data sets with $p = 500$ and 1000 nm, respectively, as shown in Fig. 5. Future theoretical works should try to evaluate L_c^* directly from Monte Carlo simulations of realistic two-dimensional geometries.

APPENDIX B

Figure 6 shows the sensitivity of the MFP spectra to the various fitting parameters in Eq. (2). The functional form of

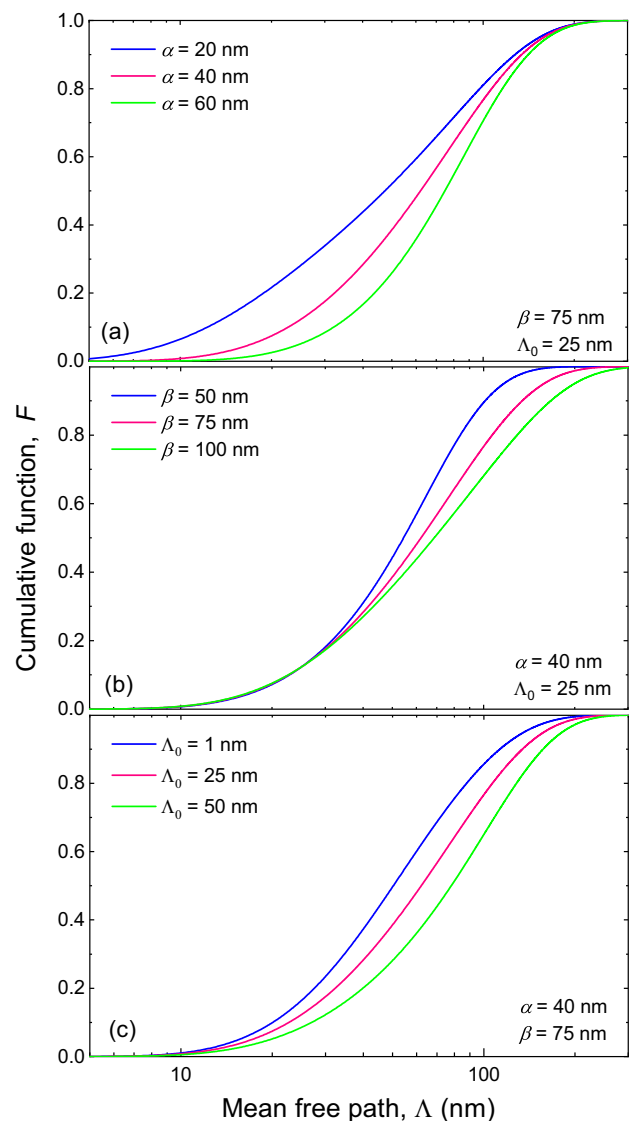


FIG. 6. Cumulative function F as a function of the phonon MFP for different values of the fitting parameters (a) α , (b) β , and (c) Λ_0 .

$F(\Lambda)$ in Eq. (2) was chosen because of two reasons: First, this function was derived by taking into account rigorous statistical considerations for a monotonic increase between 0 and 1, as detailed in Ref. [22]. Second, the three parameters α , β , and Λ_0 of $F(\Lambda)$ drive its respective changes at short, long, and intermediate ranges of the MFP spectra. Thus, Eq. (2) enables us to accurately describe the features of a cumulative function in the whole interval of MFPs. Moreover, note that the general behavior of $F(\Lambda)$ cannot be reproduced by one or two parameters, and multiple combinations of these three parameters are not expected to provide similar fits to the experimental data.

[1] K. T. Regner, J. P. Freedman, and J. A. Malen, Advances in studying phonon mean-free-path-dependent contributions to

thermal conductivity, *Nanoscale Microscale Thermophys. Eng.* **19**, 183 (2015).

- [2] J. P. Freedman, J. H. Leach, E. A. Preble, Z. Sitar, R. F. Davis, and J. A. Malen, Universal phonon mean free path spectra in crystalline semiconductors at high temperature, *Sci. Rep.* **3**, 2963 (2013).
- [3] K. T. Regner, D. P. Sellan, Z. Su, C. H. Amon, A. J. McGaughey, and J. A. Malen, Broadband phonon mean free path contributions to thermal conductivity measured using frequency domain thermoreflectance, *Nat. Commun.* **4**, 1640 (2013).
- [4] P. Jiang, L. Lindsay, and Y. K. Koh, The role of low-energy phonons with mean-free-paths $> 0.8 \mu\text{m}$ in heat conduction in silicon, *J. Appl. Phys.* **119**, 245705 (2016).
- [5] L. Zeng, K. C. Collins, Y. Hu, M. N. Luckyanova, A. A. Maznev, S. Huberman, V. Chiloyan, J. Zhou, X. Huang, K. A. Nelson, and G. Chen, Measuring phonon mean free path distributions by probing quasiballistic phonon transport in grating nanostructures, *Sci. Rep.* **5**, 17131 (2015).
- [6] Y. Hu, L. Zeng, A. J. Minnich, M. S. Dresselhaus, and G. Chen, Spectral mapping of thermal conductivity through nanoscale ballistic transport, *Nat. Nanotechnol.* **10**, 701 (2015).
- [7] A. J. Minnich, J. A. Johnson, A. J. Schmidt, K. Esfarjani, M. S. Dresselhaus, K. A. Nelson, and G. Chen, Thermal Conductivity Spectroscopy Technique to Measure Phonon Mean Free Paths, *Phys. Rev. Lett.* **107**, 095901 (2011).
- [8] M. Maldovan, Micro to nano scale thermal energy conduction in semiconductor thin films, *J. Appl. Phys.* **110**, 034308 (2011).
- [9] M. Asheghi, Y. K. Leung, S. S. Wong, and K. E. Goodson, Phonon-boundary scattering in thin silicon layers, *Appl. Phys. Lett.* **71**, 1798 (1997).
- [10] X. Wang and B. Huang, Computational study of in-plane phonon transport in Si thin films, *Sci. Rep.* **4**, 6399 (2014).
- [11] A. Malhotra and M. Maldovan, Surface scattering controlled heat conduction in semiconductor thin films, *J. Appl. Phys.* **120**, 204305 (2016).
- [12] A. Jain, Y.-J. Yu, and A. J. H. McGaughey, Phonon transport in periodic silicon nanoporous films with feature sizes greater than 100 nm, *Phys. Rev. B* **87**, 195301 (2013).
- [13] Q. Hao, Y. Xiao, and Q. Chen, Determining phonon mean free path spectrum by ballistic phonon resistance within a nanoslot-patterned thin film, *Mater. Today Phys.* **10**, 100126 (2019).
- [14] R. Anufriev, S. Gluchko, S. Volz, and M. Nomura, Quasi-ballistic heat conduction due to Lévy phonon flights in silicon nanowires, *ACS Nano* **12**, 11928 (2018).
- [15] A. George, R. Yanagisawa, R. Anufriev, J. He, N. Yoshie, S. Volz, and M. Nomura, Thermoelectric enhancement of silicon membranes by ultrathin amorphous films, *ACS Appl. Mater. Interfaces* **11**, 12027 (2019).
- [16] R. Anufriev, A. Ramiere, J. Maire, and M. Nomura, Heat guiding and focusing using ballistic phonon transport in phononic nanostructures, *Nat. Commun.* **8**, 15505 (2017).
- [17] P. Jiang, L. Lindsay, X. Huang, and Y. K. Koh, Interfacial phonon scattering and transmission loss in $> 1 \mu\text{m}$ thick silicon-on-insulator thin films, *Phys. Rev. B* **97**, 195308 (2018).
- [18] M. Verdier, D. Lacroix, S. Didenko, J.-F. F. Robillard, E. Lampin, T.-M. M. Bah, and K. Termentzidis, Influence of amorphous layers on the thermal conductivity of phononic crystals, *Phys. Rev. B* **97**, 115435 (2018).
- [19] R. Anufriev, S. Gluchko, S. Volz, and M. Nomura, Probing ballistic thermal conduction in segmented silicon nanowires, *Nanoscale* **11**, 13407 (2019).
- [20] L. Zeng, V. Chiloyan, S. Huberman, A. A. Maznev, J.-P. M. Peraud, N. G. Hadjiconstantinou, K. A. Nelson, and G. Chen, Monte Carlo study of non-diffusive relaxation of a transient thermal grating in thin membranes, *Appl. Phys. Lett.* **108**, 063107 (2016).
- [21] Y. C. Hua and B. Y. Cao, Anisotropic heat conduction in two-dimensional periodic silicon nanoporous films, *J. Phys. Chem. C* **121**, 5293 (2017).
- [22] J. Ordonez-Miranda, Y. Ezzahri, K. Joulain, J. Drevillon, and J. J. Alvarado-Gil, Modeling of the electrical conductivity, thermal conductivity, and specific heat capacity of VO₂, *Phys. Rev. B* **98**, 075144 (2018).
- [23] K. Esfarjani, G. Chen, and H. T. Stokes, Heat transport in silicon from first-principles calculations, *Phys. Rev. B* **84**, 085204 (2011).
- [24] B. Graczykowski, A. El Sachat, J. S. Reparaz, M. Sledzinska, M. R. Wagner, E. Chavez-Angel, Y. Wu, S. Volz, Y. Wu, F. Alzina, and C. M. Sotomayor Torres, Thermal conductivity and air-mediated losses in periodic porous silicon membranes at high temperatures, *Nat. Commun.* **8**, 415 (2017).
- [25] M. Nomura, J. Shiomi, T. Shiga, and R. Anufriev, Thermal phonon engineering by tailored nanostructures, *Jpn. J. Appl. Phys.* **57**, 080101 (2018).
- [26] R. Anufriev, J. Maire, and M. Nomura, Reduction of thermal conductivity by surface scattering of phonons in periodic silicon nanostructures, *Phys. Rev. B* **93**, 045411 (2016).
- [27] J. Maire, R. Anufriev, R. Yanagisawa, A. Ramiere, S. Volz, and M. Nomura, Heat conduction tuning using the wave nature of phonons, *Sci. Adv.* **3**, e1700027 (2017).
- [28] M. R. Wagner, B. Graczykowski, J. S. Reparaz, A. El Sachat, M. Sledzinska, F. Alzina, and C. M. Sotomayor Torres, Two-dimensional phononic crystals: Disorder matters, *Nano Lett.* **16**, 5661 (2016).
- [29] J. Lee, W. Lee, G. Wehmeyer, S. Dhuey, D. L. Olynick, S. Cabrini, C. Dames, J. J. Urban, and P. Yang, Investigation of phonon coherence and backscattering using silicon nanomeses, *Nat. Commun.* **8**, 14054 (2017).
- [30] J. A. Johnson, A. A. Maznev, J. Cuffe, J. K. Eliason, A. J. Minnich, T. Kehoe, C. M. S. Torres, G. Chen, and K. A. Nelson, Direct Measurement of Room-Temperature Nondiffusive Thermal Transport Over Micron Distances in a Silicon Membrane, *Phys. Rev. Lett.* **110**, 025901 (2013).
- [31] N. K. Ravichandran, H. Zhang, and A. J. Minnich, Spectrally Resolved Specular Reflections of Thermal Phonons from Atomically Rough Surfaces, *Phys. Rev. X* **8**, 041004 (2018).
- [32] A. Tavakoli, K. Lulla, T. Crozes, N. Mingo, E. Collin, and O. Bourgeois, Heat conduction measurements in ballistic 1D phonon waveguides indicate breakdown of the thermal conductance quantization, *Nat. Commun.* **9**, 4287 (2018).
- [33] N. Zen, T. A. Puurtinen, T. J. Isotalo, S. Chaudhuri, and I. J. Maasilta, Engineering thermal conductance using a two-dimensional phononic crystal, *Nat. Commun.* **5**, 3435 (2014).
- [34] Y. Tian, T. A. Puurtinen, Z. Geng, and I. J. Maasilta, Minimizing Coherent Thermal Conductance by Controlling the Periodicity of Two-Dimensional Phononic Crystals, *Phys. Rev. Appl.* **12**, 014008 (2019).
- [35] X. Huang, S. Gluchko, R. Anufriev, S. Volz, and M. Nomura, Thermal conductivity reduction in a silicon thin film with nanocones, *ACS Appl. Mater. Interfaces* **11**, 34394 (2019).